Received: 6 October 2022 | Accepted: 14 November 2022

DOI: 10.1002/pamm.202200103

A comparison of a level set method and the method of moving asymptotes for the topology optimization of flexible components in multibody systems

Ali Azari Nejat[1,*], **Alexander Held**[1], and **Robert Seifried**[1]

[1] Institute of Mechanics and Ocean Engineering, Hamburg University of Technology, Eißendorfer Straße 42, 21073 Hamburg, Germany

The gradient-based topology optimization of flexible multibody systems is considered, where the floating frame of reference method is utilized to model the flexible components with an appropriate efficiency. Thereby, the quality of the optimization results depends, among others, on the chosen gradient calculation strategy and the applied optimization algorithm. Here, both a fully-coupled time-continuous adjoint sensitivity analysis and a weakly-coupled equivalent static load method are tested for gradient calculation. Moreover, both the method of moving asymptotes and a level set method are taken to solve the optimization problem. Different combinations of the mentioned gradient strategies and optimization algorithms are applied for the topology optimization of a flexible piston rod in a slider-crank mechanism. The corresponding results and comparisons shall be used as quality benchmarks for further studies.

1 Introduction

The method of flexible multibody systems is a well-established approach for modeling and analyzing dynamic systems, whose components perform large non-linear motions including vibrations and deformations, see [14, 20]. Assuming that the body deformations are small and linear elastic, the floating frame of reference method can be used to formulate the overall motion of involved flexible components with high efficiency, and allows the compact description of the governing equations of the flexible multibody systems, see [11, 13].

The topology optimization of flexible multibody systems is a challenging task of high interest. Currently, different fully- and weakly-coupled methods are available to provide the gradient, which can be used within a gradient-based optimization process, see also [5, 18] for different gradient strategies. In literature, the method of moving asymptotes (MMA) or level set methods (LSM-s) are typically used to perform gradient-based optimization of flexible multibody systems, see [17] for the MMA-algorithm and [3] for a review of level set methods. For instance, in [6, 8, 10], MMA-based weakly- and fully-coupled topology optimization of flexible components in multibody systems are studied. Besides, in [19], a fully-coupled shape optimization and in [16] a weakly-coupled topology optimization of flexible multibody systems based on level set methods are proposed, where the design boundaries are described by the zero isosurface of a level set function defined over the design domain. Nevertheless, little is known about the benefits and drawbacks of weakly- and fully-coupled optimizations of flexible multibody systems solved by MMA- and level set-based algorithms. To this end, in the current work, the MMA-algorithm from [17] and a modified level set algorithm from [1, 21] are applied for weakly- and fully-coupled compliance minimizations of a flexible piston rod in a slider-crank mechanism. The corresponding optimization results and comparisons shall help interested readers to select suited combinations of the methods in their own studies within an optimization of flexible multibody systems.

The remainder of this work is organized as follows: In Section 2, the floating frame of reference method is addressed. A time-continuous adjoint sensitivity analysis for a fully-coupled gradient calculation and an equivalent static load method for a weakly-coupled gradient calculation are briefly described in Section 3. The application example is introduced in Section 4. The optimization results are presented in Section 5. Lastly, Section 6 concludes with a summary of this work.

2 Floating frame of reference method

In the floating frame of reference method, the deformation is captured in a body-related reference frame, which in turn undergoes large rigid body motions. Using a global Ritz approach, the elastic deformation $\boldsymbol{u}_\mathrm{P}$ for an arbitrary point P on the elastic body can be approximated as

$$\boldsymbol{u}_\mathrm{P} \approx \boldsymbol{\Phi}_\mathrm{P} \boldsymbol{q}_\mathrm{e}, \tag{1}$$

where the matrix $\boldsymbol{\Phi}_\mathrm{P}$ gathers the position-dependent global shape functions and $\boldsymbol{q}_\mathrm{e}$ is the vector of time-dependent elastic coordinates. The global shape functions can, for instance, be obtained by a model order reduction from the underlying finite element (FE-) model of the corresponding flexible components, see [12]. For an appropriate accuracy in modeling and analyzing flexible multibody systems, often a finely discretized finite element model of the flexible component is considered,

* Corresponding author: e-mail ali.azari@tuhh.de, phone +49 40 428 782 742, fax +49 40 427 314 601

which can also be reused within a topology optimization process. An appropriate choice of the global shape functions then allows for an efficient inclusion of the flexible components in the multibody simulation model and a compact formulation of the corresponding equations of motion.

3 Fully- and weakly-coupled gradient calculation

In the current work, the integral compliance of flexible bodies over the simulation time interval $[t_0, t_1]$ is chosen as objective function. This objective function can be formulated as

$$\psi = \int_{t_0}^{t_1} \boldsymbol{U}^\top \boldsymbol{K}\, \boldsymbol{U}\, \mathrm{d}t. \tag{2}$$

Thereby, $\boldsymbol{K}$ is the global stiffness matrix and $\boldsymbol{U}$ the global vector of nodal displacements of the underlying FE-model. For the gradient calculation, a time-continuous adjoint sensitivity analysis, see [7], as a fully-coupled strategy and the equivalent static load method as a weakly-coupled gradient strategy, see [9], are applied. These methods are briefly described in the following.

In the time-continuous adjoint sensitivity analysis, the gradient $\nabla\psi$, which describes the derivatives of the objective function ψ with respect to the design variables $\boldsymbol{x} \in \mathbb{R}^n$, can be determined by variational calculus, see [2, 7]. In this work, the design space consists of density-like parameters. These design variables correspond to the material filling of n finite elements. The sought gradient results from the evaluation of the following integral function

$$\nabla\psi = \int_{t_0}^{t_1} \left(\boldsymbol{T}^x_{\mathrm{OF}} - \boldsymbol{\mu}^\top \boldsymbol{T}^x_{\mathrm{KR}} - \boldsymbol{\nu}^\top \boldsymbol{T}^x_{\mathrm{EM}} \right) \mathrm{d}t. \tag{3}$$

Here, $\boldsymbol{\mu}$ and $\boldsymbol{\nu}$ are adjoint variables, which follow from the solution of an adjoint system. Moreover, the auxiliary vector $\boldsymbol{T}^x_{\mathrm{OF}}$ and the auxiliary matrices $\boldsymbol{T}^x_{\mathrm{KR}}$ and $\boldsymbol{T}^x_{\mathrm{EM}}$ include, one after the other, the derivatives of the objective function, kinematic relation and the equations of motion with respect to the design variables $\boldsymbol{x}$. To calculate these terms, among others, the derivatives of the global shape functions and of the volume integrals of the system equations with respect to the design variables are required. The computational effort of these derivative calculations and of the gradient evaluation from Eq. (3) depends directly on the number n of design variables. Hence, an appropriate reduction of the design variables helps to lower the required computation time.

In contrast, in the utilized equivalent static load method for a weakly-coupled gradient calculation, the implicit dependencies of the objective function ψ on the design variables are not included. Instead, the dynamic response is replaced by a set of n_{esl} equivalent static load cases, which lead to the same displacements $\boldsymbol{U}'_\ell$ at the chosen time points t^{esl}_ℓ with $\ell = 1:1:n_{\mathrm{esl}}$ as the dynamic response. Here, uniformly distributed time points over the simulation time interval $[t_0, t_1]$ are taken. Considering the simplification that the equivalent static loads are constant and design independent, the approximate gradient $\nabla\psi^{\mathrm{esl}}$ with respect to a design variable x_i can in general be written as

$$\nabla\psi_i^{\mathrm{esl}} = -\frac{t_1 - t_0}{n_{\mathrm{esl}}} \sum_{\ell=1}^{n_{\mathrm{esl}}} \left(\boldsymbol{U}'^\top_\ell \frac{\partial \boldsymbol{K}}{\partial x_i} \boldsymbol{U}'_\ell \right), \tag{4}$$

see [10] for more details.

To update the design within the MMA-based optimization, the gradient $\nabla\psi$ is passed to the MMA-algorithm, whereas in the considered level set algorithm, the negative gradient $\widetilde{\nabla}\psi := -\nabla\psi$ is used.

4 Application example

As an application example, a planar flexible slider-crank mechanism is considered, see Fig. 1. Similar examples can be found in [7, 8, 10, 16, 19]. Here, the mechanism consists of a rigid crank with an effective length of 100 mm, a flexible piston rod with dimensions $(400 \times 40 \times 10)$ mm and density $\rho_0 = 8750\,\mathrm{kg/m^3}$, as well as a piston with mass $m = 0.1\,\mathrm{kg}$. The flexible rod is discretized by 200×20 planar bilinear elements. The interface elements of the flexible rod are assumed as rigid, and its design domain consists of 198×20 inner elements with a reference Young's modulus of $E_0 = 50\,\mathrm{GPa}$ and a Poisson's ratio of $\nu = 0.3$. It should be noticed that the studied slider-crank mechanism is assumed to move horizontally such that the gravity is not involved. Moreover, the mass and inertia moment of the rigid crank have no influence on the dynamics of the modeled system. For this reason, these component properties are not specified here.

In the transient analysis, the system motion of the flexible slider-crank mechanism is considered within a time period of $T = 2\,\mathrm{s}$. Thereby, the rigid crank starts at $t_0 = 0\,\mathrm{s}$ from the rest position with the angle $\varphi(0) = 0\,\mathrm{rad}$, the angular velocity $\dot{\varphi}(0) = 0\,\mathrm{rad/s}$, and is continuously accelerated with a prescribed acceleration $\ddot{\varphi}(t)$ until it reaches the angular position $\varphi(2) = 12\pi\,\mathrm{rad}$ and the angular velocity $\dot{\varphi}(2) = 12\pi\,\mathrm{rad/s}$ at $t_1 = 2\,\mathrm{s}$. In Fig. 2, $\varphi(t)$, $\dot{\varphi}(t)$ and $\ddot{\varphi}(t)$ are shown.

It is worth mentioning that all implementations included in this work are carried out using MATLAB, and the corresponding calculations are performed on a personal computer equipped with a 3.80 GHz Intel® Xeon® E3 − 1270 v6 processor and 64 GB RAM.

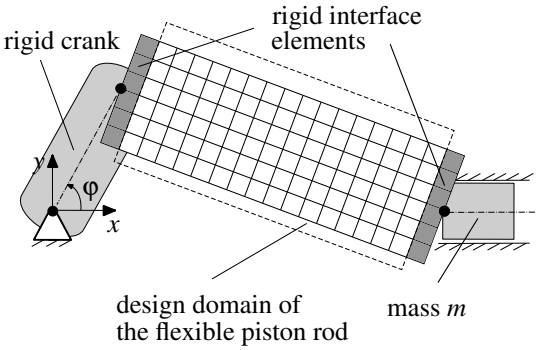

Fig. 1: Flexible slider-crank mechanism

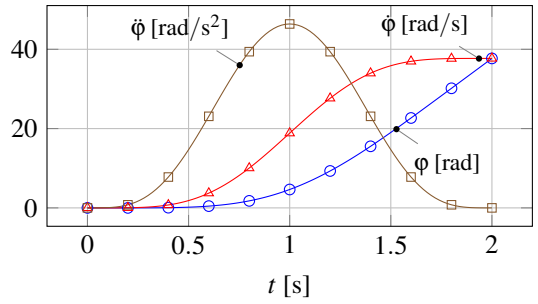

Fig. 2: Crank motion

Both the continuous adjoint sensitivity analysis and the equivalent static load method are tested for the gradient calculation within optimization processes of the flexible piston rod. As an example, the negative gradients $\widetilde{\nabla}\psi$ and $\widetilde{\nabla}\psi^{\mathrm{esl}}$ for the completely filled flexible rod, see Fig. 3, are calculated and shown in Fig. 4. Thereby, each node i on the surface plot corresponds to the gradient value with respect to the i-th design variable. The larger the negative gradient, the greater is the role of element i in compliance minimization. On the contrary, the smaller the negative gradient $\widetilde{\nabla}\psi_i$, the lower is the contribution of element i in the studied optimization problem.

It can be seen that the obtained gradients $\widetilde{\nabla}\psi$ and $\widetilde{\nabla}\psi^{\mathrm{esl}}$ are not similar. The negative gradient $\widetilde{\nabla}\psi$ obtained by the fully-coupled gradient calculation includes the influence of design variables on the compliance caused by both structural inertia and elasticity changes. Consequently, in Fig. 4a elements with a negative gradient $\widetilde{\nabla}\psi$ bigger than 0 have a higher stiffness contribution than costs caused by their inertia, whereas the elements with a negative gradient $\widetilde{\nabla}\psi$ smaller than 0 are rather likely to increase the compliance. In contrast, the negative gradient $\widetilde{\nabla}\psi^{\mathrm{esl}}$ from Fig. 4b includes only the dependency of the compliance on a change of global stiffness matrix $\boldsymbol{K}$. Hence, in this weakly-coupled case, the negative gradient $\widetilde{\nabla}\psi_i$ of each element is bigger than 0. This simplification of gradient calculation decreases the quality of optimization results. The corresponding optimization examples are shown in the following.

Fig. 3: Flexible piston rod with a completely filled design domain

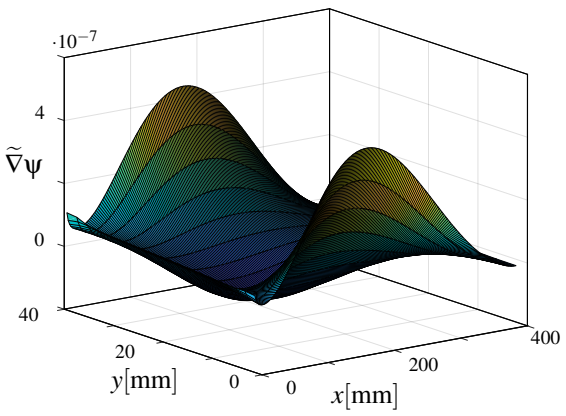

(a) Negative gradient $\widetilde{\nabla}\psi$ using fully-coupled gradient calculation

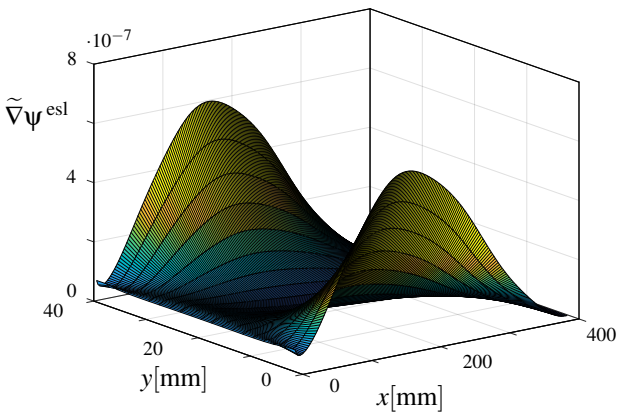

(b) Negative gradient $\widetilde{\nabla}\psi^{\mathrm{esl}}$ using weakly-coupled gradient calculation

Fig. 4: Negative gradients of the completely filled flexible piston rod over the design domain

5 Optimization results

In the current work, the fully-coupled level set-based optimization (example A), the weakly-coupled level set-based optimization (example B), the fully-coupled MMA-based optimization (example C) and the weakly-coupled MMA-based optimization (example D) of the flexible piston rod are performed and compared. It is worth mentioning that in all examples, the underlying FE-model of the flexible piston rod is parametrized by a modified solid isotropic material with penalization (SIMP) law, see [4]. Hence, a comparison of the results is valid.

In all examples, the volume limit $v_{\max}$ is set to 0.4, and the design is developed within a chosen number $n_{\mathrm{I}} = 100$ of optimization iterations. The level set-based optimizations in the examples A and B start with a completely filled initial design with a volume fraction $v_0 = 1$, whereas the MMA-based optimization in examples C and D starts from a homogeneous grey initial design with the volume fraction $v_0 = v_{\max}$. It should be noticed that the chosen initial designs in this work are the most general cases without any preconditioning. Though, there are no limitations on the choice of other initial designs.

The optimization histories of the mentioned examples are shown in Fig. 5. The greyscale element-wise representation of the final designs is given in Fig. 6, where the grey elements are those with a material filling between 0 and 1. Besides, the corresponding problem definitions and optimization results are summarized in Tab. 1.

Among the studied examples, the final designs of the fully-coupled optimizations possess the lowest final compliances, namely $\psi_{\mathrm{end}} = 0.048\,\mathrm{Nmm}$ (example A) and $\psi_{\mathrm{end}} = 0.049\,\mathrm{Nmm}$ (example C). Compared to these examples, the weakly-coupled optimizations in examples B and D provide final designs of lower quality. In example B, a final design with a compliance $\psi_{\mathrm{end}} = 0.057\,\mathrm{Nmm}$ and in example D, a final design of high greyness with $\psi_{\mathrm{end}} = 0.073\,\mathrm{Nmm}$ is reached. Moreover, the development of the volume fraction v in level set-based optimization examples A and B is different from MMA-based optimization examples C and D, see Fig. 5b. In the examples A and B, an augmented Lagrangian method is used, see also [1, 21]. This method allows to start with a volume fraction $v_0 = 1$ far away from the volume limit $v_{\max}$, and drives the optimization process towards $v_{\max}$. In contrast, the utilized MMA in the examples C and D includes a Lagrange-multiplier, which keeps the volume fraction v in the whole optimization process less than or equal to the volume limit $v_{\max}$. Despite different implementations of the volume constraint, the optimization in all 4 examples converges to similar volume fractions.

It is known that the greyness in a level set-based topology optimization is limited to elements intersected by the zero level set, whereas a standard SIMP optimization normally leads to a higher number of grey elements. This difference can qualitatively be seen in the final designs in Fig. 6, which speaks in favor of less grey final designs of examples A and B using the level set algorithm. Besides, for a quantitative comparison, the normalized greyness $\bar{g}$ can be defined as

$$\bar{g} = \frac{1}{n} \sum_{i=1}^{n} 4 x_i (1 - x_i). \tag{5}$$

see also [15]. In Fig. 5c, the greyness histories of the mentioned examples are shown. In the examples A and B, the greyness is in the beginning equal to 0, then increases slightly with the creation of new boundaries, and reaches moderate final values, namely $\bar{g}_{\mathrm{end}} = 0.12$ in example A and $\bar{g}_{\mathrm{end}} = 0.14$ in example B. In contrast, in example C and D, the MMA-based optimization starts with a greyness close to 1. The greyness then decreases during the optimization process, and reaches $\bar{g}_{\mathrm{end}} = 0.21$ in example C and $\bar{g}_{\mathrm{end}} = 0.47$ in example D, which is clearly higher than the greyness of the final designs obtained by the level set algorithm. It should be noticed that the slow convergence history and the poor final result in example D are due to the described simplification included in the weakly-coupled gradient calculation and its combination with the MMA algorithm.

Next to the different qualities of the results obtained in the mentioned examples, the corresponding computational efforts are also significantly different. Compared to the weakly-coupled gradient calculation, the fully-coupled variant is of a higher complexity. Thereby, among others, the derivatives of the system matrices and, in particular, of the global shape functions with respect to the design variables are required, whose calculation is CPU consuming. However, level set-based optimization algorithms give a simple possibility to reduce the computational effort in the fully-coupled gradient calculation. In level set-based optimizations, the boundaries between solid and void areas are implicitly given by the level set function. Since the gradient of elements in the void areas is not required to develop the design, they can be excluded from the gradient calculation in each optimization iteration. In this way, the computational effort can be reduced. The fully-coupled level set-based topology optimization in example A with the mentioned savings takes 280 min, whereas the standard MMA-based optimization in example C takes 403 min. On the other hand, the weakly-coupled optimization takes 50 min in example B and 46 min in example D. It can be argued that the presented fully-coupled optimizations A and C provide results of higher quality, whereas the weakly-coupled cases B and D are of lower computational effort.

6 Conclusion

In this work, fully- and weakly-coupled topology optimizations of flexible multibody systems are studied. Thereby, the floating frame of reference method is used to model the flexible components. An adjoint sensitivity analysis is utilized for a fully-coupled gradient calculation, and an equivalent static load method is employed for a weakly-coupled gradient calculation. These two gradient strategies are combined with both an MMA- and a level set algorithm to test different optimization procedures of flexible multibody systems. As testing example, a compliance minimization of a flexible piston rod in a planar

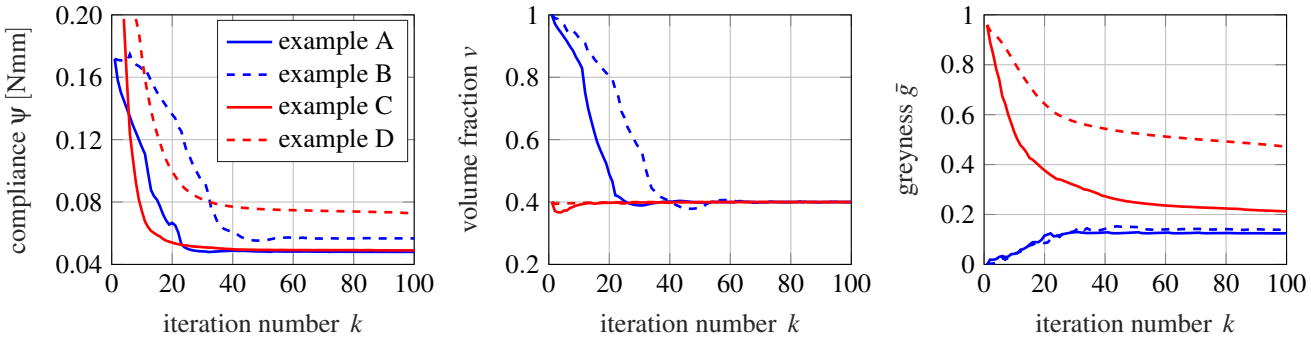

(a) Compliance **(b)** Volume **(c)** Normalized greyness

Fig. 5: Optimization histories of demonstration examples A, B, C and D

ψ_{end}=0.048 Nmm, v_{end}=0.400, $\bar{g}_{end}$=0.12

(a) Final design using fully-coupled gradient calculation and level set method - example A

ψ_{end}=0.049 Nmm, v_{end}=0.400, $\bar{g}_{end}$=0.21

(c) Final design using fully-coupled gradient calculation and method of moving asymptotes - example C

ψ_{end}=0.057 Nmm, v_{end}=0.400, $\bar{g}_{end}$=0.14

(b) Final design using weakly-coupled gradient calculation and level set method - example B

ψ_{end}=0.073 Nmm, v_{end}=0.400, $\bar{g}_{end}$=0.47

(d) Final design using weakly-coupled gradient calculation and method of moving asymptotes - example D

Fig. 6: Final designs of demonstration examples A, B, C and D

Table 1: Problem definitions and optimization results of demonstration examples A, B, C and D

Example	A	B	C	D
Optimization approach	LSM	LSM	MMA	MMA
Coupling strategy	fully-coupled	weakly-coupled	fully-coupled	weakly-coupled
Width/length ratio (FE-discretization)	1/10 (20×200)	1/10 (20×200)	1/10 (20×200)	1/10 (20×200)
Volume limit v_{max}	0.4	0.4	0.4	0.4
Successful iterations n_s	100	100	100	100
Final compliance ψ_{end} [Nmm]	0.048	0.057	0.049	0.073
Final volume fraction v_{end}	0.400	0.400	0.400	0.400
Final greyness $\bar{g}_{end}$	0.12	0.14	0.21	0.47
Computation time [min]	280	50	403	46

slider-crank mechanism is used. The optimization results reveal, among others, some benefits of level set-based optimizations compared to the MMA-based ones. In general, the level set-based optimization results are of lower greyness. The weakly-coupled level set-based optimization converges faster and reaches a significantly smaller final compliance than in the MMA-based case. Besides, in the level set-based optimization, grey elements arise only around the boundaries, and the void elements can be simply excluded from the gradient calculation. This helps to reduce the computational effort of a CPU-intensive adjoint sensitivity analysis in the fully-coupled optimization case.

Acknowledgements The authors would like to thank the German Research Foundation (DFG) for financial support of this work within a research project with the number 421344187. Open access funding enabled and organized by Projekt DEAL.

References

[1] Azari Nejat, A., Held, A., Trekel, N., Seifried, R.: A modified level set method for topology optimization of sparsely-filled and slender structures. Structural and Multidisciplinary Optimization **65**(3), 1–22 (2022)

[2] Bestle, D., Seybold, J.: Sensitivity analysis of constrained multibody systems. Archive of Applied Mechanics **62**(3), 181–190 (1992)

[3] van Dijk, N.P., Maute, K., Langelaar, M., van Keulen, F.: Level-set methods for structural topology optimization: a review. Structural and Multidisciplinary Optimization **48**(3), 437–472 (2013)

[4] Du, J., Olhoff, N.: Topological design of freely vibrating continuum structures for maximum values of simple and multiple eigenfrequencies and frequency gaps. Structural and Multidisciplinary Optimization **34**(2), 91–110 (2007)

[5] Gufler, V., Wehrle, E., Zwölfer, A.: A review of flexible multibody dynamics for gradient-based design optimization. Multibody System Dynamics **53**(4), 379–409 (2021)

[6] Held, A., Knüfer, S., Seifried, R.: Topology optimization of members of dynamically loaded flexible multibody systems using integral type objective functions and exact gradients. In: 11th World Congress on Structural and Multidisciplinary Optimization, pp. 7–12. Sydney Australia (2015)

[7] Held, A., Knüfer, S., Seifried, R.: Structural sensitivity analysis of flexible multibody systems modeled with the floating frame of reference approach using the adjoint variable method. Multibody System Dynamics **40**(3), 287–302 (2017)

[8] Held, A., Nowakowski, C., Moghadasi, A., Seifried, R., Eberhard, P.: On the influence of model reduction techniques in topology optimization of flexible multibody systems using the floating frame of reference approach. Structural and Multidisciplinary Optimization **53**(1), 67–80 (2016)

[9] Kang, B.S., Park, G.J., Arora, J.S.: Optimization of flexible multibody dynamic systems using the equivalent static load method. AIAA Journal **43**(4), 846–852 (2005)

[10] Moghadasi, A., Held, A., Seifried, R.: Topology optimization of members of flexible multibody systems under dominant inertia loading. Multibody System Dynamics **42**(4), 431–446 (2018)

[11] Schwertassek, R., Wallrapp, O.: Dynamik flexibler Mehrkörpersysteme: Methoden der Mechanik zum rechnergestützten Entwurf und zur Analyse mechatronischer Systeme. Grundlagen und Fortschritte der Ingenieurwissenschaften. Vieweg+Teubner Verlag (1999)

[12] Schwertassek, R., Wallrapp, O., Shabana, A.A.: Flexible multibody simulation and choice of shape functions. Nonlinear dynamics **20**(4), 361–380 (1999)

[13] Seifried, R.: Dynamics of underactuated multibody systems: Modeling, control and optimal design. Solid Mechanics and Its Applications. Springer Science & Business Media (2013)

[14] Shabana, A.A.: Flexible multibody dynamics: Review of past and recent developments. Multibody System Dynamics **1**(2), 189–222 (1997)

[15] Sigmund, O.: Morphology-based black and white filters for topology optimization. Structural and Multidisciplinary Optimization **33**(4-5), 401–424 (2007)

[16] Sun, J., Tian, Q., Hu, H.: Topology optimization based on level set for a flexible multibody system modeled via ANCF. Structural and Multidisciplinary Optimization **55**(4), 1159–1177 (2017)

[17] Svanberg, K.: The method of moving asymptotes — a new method for structural optimization. International Journal for Numerical Methods in Engineering **24**(2), 359–373 (1987)

[18] Tromme, E., Held, A., Duysinx, P., Brüls, O.: System-based approaches for structural optimization of flexible mechanisms. Archives of Computational Methods in Engineering **25**(3), 817–844 (2018)

[19] Tromme, E., Tortorelli, D., Brüls, O., Duysinx, P.: Structural optimization of multibody system components described using level set techniques. Structural and Multidisciplinary Optimization **52**(5), 959–971 (2015)

[20] Wasfy, T.M., Noor, A.K.: Computational strategies for flexible multibody systems. Applied Mechanics Reviews **56**(6), 553–613 (2003)

[21] Wei, P., Li, Z., Li, X., Wang, M.Y.: An 88-line MATLAB code for the parameterized level set method based topology optimization using radial basis functions. Structural and Multidisciplinary Optimization **58**(2), 831–849 (2018)